

A NOTE ON ROBUST PRECONDITIONERS FOR MONOLITHIC FLUID-STRUCTURE INTERACTION SYSTEMS OF FINITE ELEMENT EQUATIONS

ULRICH LANGER AND HUIDONG YANG

ABSTRACT. In this note, we consider preconditioned Krylov subspace methods for discrete fluid-structure interaction problems with a nonlinear hyperelastic material model and covering a large range of flows, e.g., water, blood, and air with highly varying density. Based on the complete LDU factorization of the coupled system matrix, the preconditioner is constructed in form of $\hat{L}\hat{D}\hat{U}$, where \hat{L} , \hat{D} and \hat{U} are proper approximations to L , D and U , respectively. The inverse of the corresponding Schur complement is approximated by applying one cycle of a special class of algebraic multigrid methods to the perturbed fluid sub-problem, that is obtained by modifying corresponding entries in the original fluid matrix with an explicitly constructed approximation of the exact perturbation coming from the sparse matrix-matrix multiplications.

1. MOTIVATION

During the past years, robust and efficient monolithic fluid-structure interaction (FSI) solvers attract a lot of interests from many researchers; see, e.g., [13, 29, 18, 16, 4, 9, 6], that are mainly based on algebraic multigrid (AMG) [30], geometry multigrid (GMG) [15], preconditioned Krylov subspace [32] and domain decomposition (DD) [28, 35] methods. In our previous work [23], we implemented FSI monolithic AMG solvers with the W-cycle and with a variant of the W-cycle, i.e., a recursive Krylov-based multigrid cycle, somehow related to the algebraic multilevel method, see, e.g., [2, 3, 20, 22, 37, 27, 1], as well as their corresponding preconditioners for the coupled FSI problem using the AMG preconditioners [21, 14, 38, 24] for each sub-problem in the smoothing steps. In addition, we also considered the preconditioned GMRES method (see [33]), using a class of block-wise Gauss-Seidel type preconditioners (see the earlier work in [13]), that are based on the aforementioned AMG methods for the sub-problems. As well known, such block-wise Gauss-Seidel preconditioned Krylov subspace methods may lose the robustness with respect to the mesh size, i.e., the iteration numbers for solving the coupled FSI system nearly double,

when the mesh size halves; see the numerical results in our previous work [23]. In this work, we further observe, that the methods are not robust with respect to the varying fluid density. For an illustration, we have tested the methods on the numerical example given in Section 4, where the fluid density is varying (from water to air flow): $\rho_f \in \{1.1, 0.11, 0.011, 0.0011\}$ g/cm³. The preconditioners employed in the preconditioned GMRES method are: The block diagonal (\tilde{P}_D), the block lower triangular (\tilde{P}_L), the block upper triangular (\tilde{P}_U), the SSOR (\tilde{P}_{SSOR}) and the $ILU(0)$ (\tilde{P}_{ILU}); see the definition in [23]. The number of iterations (#it) for solving the linearized FSI system on the coarse mesh using the time step size $\Delta t = 0.125$ ms is displayed in Table 1. As observed, the preconditioned Krylov subspace methods do not

ρ_f	#it				
	1.1	0.11	0.011	0.0011	0.00011
\tilde{P}_D	57	185	> 250	> 250	> 250
\tilde{P}_L	38	68	89	112	> 250
\tilde{P}_U	38	68	81	92	> 250
\tilde{P}_{SSOR}	38	68	108	82	114
\tilde{P}_{ILU}	38	68	83	82	74

TABLE 1. The number of iterations of the preconditioned GMRES method for solving the coupled FSI system with varying fluid density $\rho_f \in \{1.1, 0.11, 0.011, 0.0011, 0.00011\}$ g/cm³.

show the robustness with respect to the varying fluid density, i.e., the iteration numbers grow more or less when the fluid density decreases. In addition, the iteration numbers in the first column correspond to the numerical results in [23], where a similar fluid density has been adopted. Note that, here we stop the linear solver when the error in the GMRES iteration is reduced by a factor of 10^{10} . The numerical results are shown for the first Newton iteration.

Although we are able to cure the mesh dependence issue by using the fully coupled monolithic AMG methods, provided we have designed effective smoothers and coarsening strategies for such multifield problems, this task in general turns out to be nontrivial, see, e.g., [13].

Motivated by the above observations, in this work, we aim to construct a more robust and efficient preconditioner in preconditioned Krylov subspace methods for the monolithic coupled FSI system, that

is based on the approximation of the direct complete LDU factorization of the coupled system matrix.

The remainder of paper is organized as follows. In Section 2, we set up a FSI model problem for testing our methods. Section 3 deals with the construction of the robust and efficient preconditioner in Krylov subspace methods for the linearized and discretized model problem. Numerical studies are presented in Section 4. Finally, some conclusions are drawn in Section 5.

2. A MODEL FSI PROBLEM AND ITS DISCRETIZATION

2.1. The geometrical configuration, mappings and kinematics.

We consider the FSI domain Ω^t as a union of the deformable fluid domain Ω_f^t and structure domain Ω_s^t at the time t : $\bar{\Omega}^t := \bar{\Omega}_f^t \cup \bar{\Omega}_s^t$ and $\Omega_f^t \cap \Omega_s^t = \emptyset$. The boundary of the fluid domain $\partial\Omega_f^t$ is decomposed into several parts: $\partial\Omega_f^t := \bar{\Gamma}_{in} \cup \bar{\Gamma}_{out} \cup \bar{\Gamma}_{wall} \cup \bar{\Gamma}^t$ and $\Gamma_{in} \cap \Gamma_{out} = \Gamma_{in} \cap \Gamma_{wall} = \Gamma_{in} \cap \Gamma^t = \Gamma_{out} \cap \Gamma_{wall} = \Gamma_{out} \cap \Gamma^t = \emptyset$. In an analogous way, the boundary $\partial\Omega_s^t$ of the structure domain is decomposed into the following parts: $\partial\Omega_s^t := \bar{\Gamma}_d \cup \bar{\Gamma}_n^t \cup \bar{\Gamma}^t$ and $\Gamma_d \cap \Gamma_n^t = \Gamma_d \cap \Gamma^t = \Gamma_n^t \cap \Gamma^t = \emptyset$. The interface Γ^t is defined as the intersection of the fluid and structure boundary: $\Gamma^t := \partial\Omega_f^t \cap \partial\Omega_s^t$. At the time level $t = 0$, we have the initial (reference) configuration. See a schematic illustration in Fig. 1.

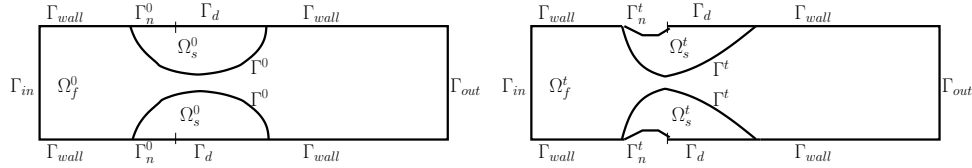


FIGURE 1. An illustration of the computational FSI domain at the initial time $t = 0$ (left) and the current time t (right).

As usual, we use the Arbitrary-Lagrangian-Eulerian (ALE) mapping defined as $\mathcal{A}^t := \mathcal{A}^t(x) = x + d_f(x, t)$, $\forall x \in \Omega_f^0$, to track the movement of the fluid domain Ω_f^0 , where the $d_f := d_f(x, t)$, $\forall x \in \Omega_f^0$ denotes the fluid domain displacement; see, e.g., [19, 12, 10]. For the structure sub-problem, the Lagrangian mapping $\mathcal{L}^t := \mathcal{L}^t(x) = x + d_s(x, t)$, $\forall x \in \Omega_s^0$ is used to track the structure body movement; see, e.g., [7, 17]. In addition, the fluid velocity $u := u(x, t)$, $\forall x \in \Omega_f^0$ and pressure $p := p(x, t)$, $\forall x \in \Omega_f^0$ are defined via the ALE mapping: $u(x, t) = \tilde{u}(\tilde{x}, t) = \tilde{u}(\mathcal{A}_f^t(x), t)$, $p(x, t) = \tilde{p}(\tilde{x}, t) = \tilde{p}(\mathcal{A}_f^t(x), t)$, $\forall x \in \Omega_f^0$ and

$\tilde{x} = \mathcal{A}_f^t(x) \in \Omega_f^t$, where $\tilde{u}(\cdot, \cdot)$ and $\tilde{p}(\cdot, \cdot)$ denote the fluid velocity and pressure variables under the Eulerian framework; see, e.g., [40].

Since we formulate the coupled FSI system on the reference configuration for the fluid sub-problem by the ALE mapping and structure sub-problem by the Lagrangian mapping, we need to introduce the necessary notations in the kinematics as used in, e.g., [7, 17]. For this, we define the fluid and structure deformation gradient tensor by $F_f := F_f(x) = \partial \mathcal{A}^t / \partial x = I + \nabla d_f$, $\forall x \in \Omega_f^0$ and $F_s := F_s(x) = \partial \mathcal{L}^t / \partial x = I + \nabla d_s$, $\forall x \in \Omega_s^0$, respectively. Their determinants are given by $J_f = \det F_f$ and $J_s = \det F_s$, accordingly.

2.2. A monolithic FSI system on the reference configuration.

After the above preliminary, we formulate the the coupled FSI system in strong form on the reference domain: Find (d_f, u, p, d_s) such that

$$(1a) \quad -\Delta d_f = 0 \quad \text{in } \Omega_f^0,$$

$$(1b) \quad d_f = d_s \quad \text{on } \Gamma^0,$$

$$(1c) \quad \begin{aligned} &\rho_f J_f \partial_t u + \rho_f J_f ((u - w_f) \cdot F_f^{-1} \nabla) u \\ &-\nabla \cdot (J_f \sigma_f(u, p) F_f^{-T}) = 0 \quad \text{in } \Omega_f^0, \end{aligned}$$

$$(1d) \quad \nabla \cdot (\rho_f J_f F_f^{-1} u) = 0 \quad \text{in } \Omega_f^0,$$

$$(1e) \quad \rho_s \partial_{tt} d_s - \nabla \cdot (F_s S) = 0 \quad \text{in } \Omega_s^0,$$

$$(1f) \quad u = \partial_t d_s \quad \text{on } \Gamma^0,$$

$$(1g) \quad J_f \sigma_f(u, p) F_f^{-T} n_f + F_s S n_s = 0 \quad \text{on } \Gamma^0.$$

To complete the system, we prescribe the corresponding boundary conditions $d_f = 0$ on $\Gamma_{in} \cup \Gamma_{wall} \cup \Gamma_{out}$, $u = 0$ on Γ_{wall} , $u = g_{in}$ (a given function) on Γ_{in} and $J_f \sigma_f(u, p) F_f^{-T} n_f = 0$ on Γ_{out} , $d_s = 0$ on Γ_d and $F_s S n_s = 0$ on Γ_n , and the proper initial conditions $u(x, 0) = 0$, $\forall x \in \Omega_f^0$ and $d_s(x, 0) = \partial_t d_s(x, 0) = 0$, $\forall x \in \Omega_s^0$.

Here, the notations ρ_f and ρ_s denote the fluid and structure density, respectively, n_f and n_s the fluid and structure outward unit normal vector, respectively, $\sigma_f(u, p) := \mu(\nabla u + \nabla^T) - pI$ the Cauchy stress tensor with the dynamic viscosity term μ .

For the structure, we use the hyperelastic model of the St. Venant Krichhoff material, for which the second Piola Kirchhoff stress tensor S is defined as

$$(2) \quad S := \lambda_s \text{tr}(E_s) I + 2\mu_s E_s$$

where $E_s := 0.5(F_s^T F_s - I)$ denotes the Green-Lagrange strain tensor with the Lamé constant λ_s and the shear modulus μ_s .

Remark 2.1. Note that, in [18, 40], a monolithic formulation was introduced and used for the FSI simulation, where the structure velocity variable is introduced to rewrite the structure equation into a system of two first order time dependent equations so that both the fluid and structure sub-problems are rewritten in a monolithic manner on the reference domain Ω^0 . In our approach, we keep the form of structure equation, but transform the fluid sub-problem onto the fluid reference domain by the ALE mapping. By this means, we keep the modulus of each sub-problem so that robust solvers for the sub-problem can be directly applied.

2.3. Temporal and spatial discretization and linearization. Concerning the temporal and spatial discretization, we follow the approaches in our previous work [24, 23]. For the time discretization of the fluid and structure sub-problem, we use the first order implicit Euler scheme and a first order Newmark- β scheme, respectively. For the spatial discretization of the fluid sub-problem, we use the stabilized $P_1 - P_1$ finite element discretization with standard hat basis functions for both the fluid velocity and pressure interpolations. For the mesh movement and structure sub-problem, we use the P_1 finite element discretization with the standard hat function for both the fluid and structure displacement interpolations. Following the approach in [23], the nonlinearity of the monolithic FSI system is handled by Newton's method.

3. MONOLITHIC SOLUTION METHODS FOR THE COUPLED FSI SYSTEM

3.1. The modified coupled FSI system. Based on our previous work [23], the linearized coupled FSI system is formulated as

$$(3) \quad \left[\begin{array}{cc|cc|cc|cc} A_m^{ii} & A_m^{i\gamma} & & & & & & \\ & I & & & & & & \\ \hline B_{fm}^i & B_{fm}^\gamma & -C_f & B_{1f}^i & B_{1f}^\gamma & & & \\ A_{fm}^{ii} & A_{fm}^{i\gamma} & B_{2f}^i & A_f^{ii} & A_f^{i\gamma} & & & \\ A_{fm}^{\gamma i} & A_{fm}^{\gamma\gamma} & B_{2f}^\gamma & A_f^{\gamma i} & A_f^{\gamma\gamma} & A_s^{\gamma\gamma} & A_s^{\gamma i} & \\ \hline & & & & -I & \frac{1}{\Delta t} I & & \\ & & & & & A_s^{i\gamma} & A_s^{ii} & \end{array} \right] \begin{bmatrix} \Delta d_m^i \\ \Delta d_m^\gamma \\ \Delta p \\ \Delta u_f^i \\ \Delta u_f^\gamma \\ \Delta d_s^\gamma \\ \Delta d_s^i \end{bmatrix} = \begin{bmatrix} r_m^i \\ r_m^\gamma \\ r_p \\ r_f^i \\ r_f^\gamma \\ r_s^\gamma \\ r_s^i \end{bmatrix},$$

where the superscript γ indicates the (nodal) degrees of freedom (DOF) associated to the variables on the interface, i denotes the remaining DOF, $\beta\alpha$, $\beta, \alpha \in \{\gamma, i\}$, $\beta \neq \alpha$ means the coupling between the corresponding interface variables and the remaining. Here the second row

corresponds to the interface coupling between the mesh movement and the structure displacement, the fifth and sixth rows correspond to the equivalence of surface tractions and the no-slip interface condition from the fluid and structure side, respectively. It is easy to see, on the main diagonal, we have stiffness matrices for the mesh movement, fluid and structure sub-problem, respectively, and the off-diagonal matrices denote the coupling among them.

In order to derive the robust preconditioner for the coupled FSI system in a convenient manner, we reorder the system (3) by changing the rows and columns, and modify some of the matrix entries and the right hand side accordingly. This way, we obtain the following equivalent linear system of equations:

$$(4) \quad \left[\begin{array}{cc|cc|ccc} A_m^{ii} & & A_{ms}^{i\gamma} & & & & \\ & I & -I & & & & \\ \hline & & A_s^{ii} & & \Delta t A_{sf}^{i\gamma} & & \\ & & & \frac{1}{\Delta t} I & -I & & \\ \hline A_{fm}^{\gamma i} & A_{fm}^{\gamma\gamma} & A_s^{\gamma i} & A_s^{\gamma\gamma} & A_f^{\gamma\gamma} & A_f^{\gamma i} & B_{2f}^{\gamma} \\ A_{fm}^{ii} & A_{fm}^{i\gamma} & & & A_f^{i\gamma} & A_f^{ii} & B_{2f}^i \\ B_{fm}^i & B_{fm}^{\gamma} & & & B_{1f}^{\gamma} & B_{1f}^i & -C_f \end{array} \right] \begin{bmatrix} \Delta d_m^i \\ \Delta d_m^{\gamma} \\ \Delta d_s^i \\ \Delta d_s^{\gamma} \\ \Delta u_f^{\gamma} \\ \Delta u_f^i \\ \Delta p \end{bmatrix} = \begin{bmatrix} \tilde{r}_m^i \\ r_m^{\gamma} \\ \tilde{r}_s^i \\ r_s^{\gamma} \\ r_f^{\gamma} \\ r_f^i \\ r_p \end{bmatrix},$$

where

$$(5) \quad \tilde{r}_m^i = r_m^i - A_m^{i\gamma} r_m^{\gamma}, \quad \tilde{r}_s^i = r_s^i - \Delta t A_s^{i\gamma} r_s^{\gamma}.$$

By this means, we keep the system matrix for the sub-problems on the diagonal as symmetric as possible to make our linear solver for the sub-problem more efficient, e.g., by applying conjugate gradient method with AMG preconditioner (see [14]). Nevertheless, keeping the symmetry of the sub-problem is not mandatory. For instance, for nonsymmetric positive systems, a class of AMG methods with special transfers base on Schur complements and Galerkin projections are proposed in the recent work [41]. On the other hand, we face the unsymmtry for the fluid sub-problem any way, mainly due to the convection and stabilization terms. This issue is handled by a class of coupled AMG methods [38, 39, 43, 42, 24].

For convenience of the following presentation, we rewrite the re-ordered system (4) in the following compact form:

$$(6) \quad Kx = b,$$

where

$$(7) \quad K = \begin{bmatrix} A_m & A_{ms} & 0 \\ 0 & A_s & A_{sf} \\ A_{fm} & A_{fs} & A_f \end{bmatrix}, \quad x = \begin{bmatrix} x_m \\ x_s \\ x_f \end{bmatrix}, \quad b = \begin{bmatrix} b_m \\ b_s \\ b_f \end{bmatrix}.$$

Here the block matrices and vectors are assigned according to the subdivision of the FSI system (4).

3.2. Construct the Schur complement approximation. To construct the Schur complement approximation of the FSI system, we start to perform a *LDU* factorization for the 3×3 block matrix K . In this case, the factorization is formulated as

$$(8) \quad \begin{aligned} K &= LDU \\ &:= \begin{bmatrix} I & 0 & 0 \\ 0 & I & 0 \\ A_{fm}A_m^{-1} & \tilde{A}_{fs}A_s^{-1} & I \end{bmatrix} \begin{bmatrix} A_m & 0 & 0 \\ 0 & A_s & 0 \\ 0 & 0 & S \end{bmatrix} \begin{bmatrix} I & A_m^{-1}A_{ms} & 0 \\ 0 & I & A_s^{-1}A_{sf} \\ 0 & 0 & I \end{bmatrix} \\ &= \begin{bmatrix} A_m & 0 & 0 \\ 0 & A_s & 0 \\ A_{fm} & \tilde{A}_{fs} & S \end{bmatrix} \begin{bmatrix} I & A_m^{-1}A_{ms} & 0 \\ 0 & I & A_s^{-1}A_{sf} \\ 0 & 0 & I \end{bmatrix}, \end{aligned}$$

where the fluid Schur complement is formulated as

$$(9) \quad S = A_f - \tilde{A}_{fs}A_s^{-1}A_{sf}$$

with

$$(10) \quad \tilde{A}_{fs} = A_{fs} - A_{fm}A_m^{-1}A_{ms}.$$

Inspired by this observation, we propose the following FSI preconditioner

$$(11) \quad \begin{aligned} \hat{K} &= \hat{L}\hat{D}\hat{U} \\ &:= \begin{bmatrix} I & 0 & 0 \\ 0 & I & 0 \\ A_{fm}\hat{A}_m^{-1} & \hat{\tilde{A}}_{fs}\hat{A}_s^{-1} & I \end{bmatrix} \begin{bmatrix} \hat{A}_m & 0 & 0 \\ 0 & \hat{A}_s & 0 \\ 0 & 0 & \hat{S} \end{bmatrix} \begin{bmatrix} I & \hat{A}_m^{-1}A_{ms} & 0 \\ 0 & I & \hat{A}_s^{-1}A_{sf} \\ 0 & 0 & I \end{bmatrix} \\ &= \begin{bmatrix} \hat{A}_m & 0 & 0 \\ 0 & \hat{A}_s & 0 \\ A_{fm} & \hat{\tilde{A}}_{fs} & \hat{S} \end{bmatrix} \begin{bmatrix} I & \hat{A}_m^{-1}A_{ms} & 0 \\ 0 & I & \hat{A}_s^{-1}A_{sf} \\ 0 & 0 & I \end{bmatrix}. \end{aligned}$$

Here the approximation of the fluid Schur complement is defined as

$$(12) \quad \hat{S} = A_f - \hat{\tilde{A}}_{fs}\hat{A}_s^{-1}A_{sf}$$

with

$$(13) \quad \hat{\hat{A}}_{fs} = A_{fs} - A_{fm} \hat{\hat{A}}_m^{-1} A_{ms},$$

where

$$(14) \quad \hat{\hat{A}}_m = \text{diag}[A_m], \quad \hat{\hat{A}}_s = \text{diag}[A_s].$$

The notation "diag" means the block diagonal of the corresponding matrix from the mesh movement and the structure sub-problem, respectively. By this means, we are able to construct the fluid Schur complement in an explicit way, that corresponds to a full fluid matrix perturbed by the matrix from the multiplication of the approximated coupling matrices of the fluid and mesh movement sub-problem, the fluid and structure sub-problem, and the structure and mesh movement sub-problem, respectively.

Remark 3.1. In principle, we can choose different approximations to A_m appearing in the \hat{L} , \hat{D} , and \hat{U} of (11). In our case, we utilize the same approximation $\hat{\hat{A}}_m$, i.e., one corresponding AMG iteration is applied to the mesh movement sub-problem for the inverse approximation. The same applies to the approximation for A_s .

Remark 3.2. To approximate A_m and A_s appearing in the fluid Schur complement (9), we employ the diagonal of the matrix as an approximation, that turns out to be a rather robust and meanwhile cheap approximation in our applications. However, in principle, the methodology here can be extended to other situations, where the approximation for the inverse of A_m and A_s can be computed explicitly in another cheap way.

Remark 3.3. The constructure of the fluid Schur complement approximation (12) turns out to be a fairly cheap operation. Since the matrices A_{fs} , A_{ms} and A_{sf} have very sparse non-zero pattern corresponding to the coupling conditions among the mesh movement, fluid and structure sub-problems on the interface only, the cost of multiplication between the matrices, and between the matrix and the diagonal of the matrix is rather cheap. In addition, the sparse matrix A_{fm} couples the mesh movement and the fluid sub-problem in the fluid reference domain. Thus, it has more entries than the interface coupling matrices. Finally, we only need to modify the entries in the A_f and B_{1f} blocks of the fluid matrix in (4) in order to construct the fluid Schur complement. By neglecting the perturbation $-A_{fm} \hat{\hat{A}}_m^{-1} A_{ms}$ in (9), a cheaper inexact approximation for the Schur complement S is obtained. However, this approximation turns out to be too rough to get the robustness of the preconditioner. Thus it will not be discussed in the following.

Remark 3.4. There are two other direct ways to construct the Schur complement for the coupled FSI system.

One way is to construct the structure Schur complement:

$$(15) \quad S = A_s - A_{sf}A_f^{-1}\tilde{A}_{fs} = A_s - A_{sf}A_f^{-1}(A_{fs} - A_{fm}A_m^{-1}A_{ms}),$$

based on the following *LDU* factorization of the original coupled system:

$$\begin{bmatrix} A_m & 0 & A_{ms} \\ A_{fm} & A_f & A_{fs} \\ 0 & A_{sf} & A_s \end{bmatrix} = \begin{bmatrix} I & 0 & 0 \\ A_{fm}A_m^{-1} & I & 0 \\ 0 & A_{sf}A_f^{-1} & I \end{bmatrix} \begin{bmatrix} A_m & 0 & 0 \\ 0 & A_f & 0 \\ 0 & 0 & S \end{bmatrix} \begin{bmatrix} I & 0 & A_m^{-1}A_{ms} \\ 0 & I & A_f^{-1}\tilde{A}_{fs} \\ 0 & 0 & I \end{bmatrix},$$

where $\tilde{A}_{fs} = A_{fs} - A_{fm}A_m^{-1}A_{ms}$.

The other way is to construct the mesh movement Schur complement:

$$(16) \quad S = A_m - A_{mf}A_{fm} = A_m + A_{ms}A_s^{-1}A_{sf}(A_f - A_{fs}A_s^{-1}A_{sf})^{-1}A_{fm},$$

based on the following *LDU* factorization of the reordered FSI system:

$$\begin{bmatrix} A_s & A_{sf} & 0 \\ A_{fs} & A_f & A_{fm} \\ A_{ms} & 0 & A_m \end{bmatrix} = \begin{bmatrix} I & 0 & 0 \\ A_{fs}A_s^{-1} & I & 0 \\ A_{ms}A_s^{-1} & A_{mf} & I \end{bmatrix} \begin{bmatrix} A_s & 0 & 0 \\ 0 & \tilde{A}_f & 0 \\ 0 & 0 & S \end{bmatrix} \begin{bmatrix} I & A_s^{-1}A_{sf} & 0 \\ 0 & I & \tilde{A}_f^{-1}A_{fm} \\ 0 & 0 & I \end{bmatrix},$$

where $\tilde{A}_f = A_f - A_{fs}A_s^{-1}A_{sf}$ and $A_{mf} = -A_{ms}A_s^{-1}A_{sf}\tilde{A}_f^{-1}$.

However, none of these two Schur complements (15) and (16) is cheaper than the fluid Schur complement (9) to approximate. From now on, we only consider the preconditioner \hat{K} constructed in (11).

3.3. The preconditioning steps. The preconditioning operation in the preconditioned Krylov subspace methods, e.g., the preconditioned GMRES [33] or the flexible preconditioned GMRES [31], requires the evaluation $x = \hat{K}^{-1}r$ for a given vector $r = [r_m^T, r_s^T, r_f^T]^T$. One inverse operation contains five steps as indicated in Algorithm 1. As observed, we need to evaluate the inverse of \hat{A}_m and \hat{A}_s applied to the corresponding vectors twice, and the inverse evaluation of the approximated fluid Schur complement \hat{S} applied to a vector once, that is the most expensive operation in the preconditioning steps. All the evaluation is computed by applying one cycle of a special class of AMG methods [21, 38, 42, 43] to the corresponding sub-problem with 0 as initial guess,

Algorithm 1 Evaluation of $x = \hat{K}^{-1}r$

- 1: $\tilde{x}_m = \hat{A}_m^{-1}r_m$,
 - 2: $\tilde{x}_s = \hat{A}_s^{-1}r_s$,
 - 3: $x_f = \hat{S}^{-1}(r_f - A_{fm}\tilde{x}_m - \hat{A}_{fs}\tilde{x}_s)$,
 - 4: $x_s = \tilde{x}_s - \hat{A}_s^{-1}A_{sf}x_f$,
 - 5: $x_m = \tilde{x}_m - \hat{A}_m^{-1}A_{ms}x_s$.
-

that turns out to be sufficient to evaluate the inverse approximation in the preconditioning steps.

3.4. Some remarks on other related preconditioners. In this subsection, we make some remarks on other known preconditioned Krylov subspace methods for the coupled FSI system. For instance, in [9, 6], the domain decomposition based additive Schwarz preconditioners have been used in the parallel FSI solvers.

Remark 3.5. In [16], the author considered the preconditioned Krylov subspace method for the FSI problem in 2D using a 1D model of the wall deformation. Starting from the three block-triangular approximations (as preconditioners) of the original linearized system, the "sup", the "sub" and the "diag", the author then used a global pressure Schur complement preconditioner [36] to replace the Navier-Stokes block, in which the Elman's *BFBt* approximation [11] to the fluid pressure Schur complement is employed in order to reduce the computational cost. Later on, in [26], the authors considered a FSI preconditioner for a 4×4 linearized FSI system by replacing the bottom-right 2×2 block in the Jacobian with the so-called pseudo-solid preconditioner. In our approach, we construct the preconditioner based the complete *LDU* factorization for the the linearized 3×3 coupled system and the approximated Schur complement itself is on the sub-problem level, corresponding to the perturbed fluid sub-problem, see (12), for which we have very efficient and robust AMG method [38, 39, 43, 24] to perform the inverse operation.

Remark 3.6. In [4], the authors considered the domain decomposition Dirichlet-Neumann, the ILU and the inexact block-LU factorization based preconditioners for the FSI system linearized by the fixed point algorithm for both the domain dependence and the convective term. Thus the linear system therein has slightly different structure as we consider in this work. Herein, more coupling matrix blocks come into the the system due to the nonlinearity of the domain movement and the convective term treated in an all-at-once manner using Newton's

method. In their inexact block-LU factorization based preconditioner, the inverse of the fluid matrix appears several times in the block structure, that is approximated by Neumann expansion technique. The similar technique was also used in [5]. In our approach, by reordering the coupled system we arrive at the fluid Schur complement, that involves the inverse of the perturbed fluid matrix only once. Furthermore, one complete preconditioning step involves the inverse of the mesh movement and structure matrices twice, that are in general cheaper to approximate than the inverse of the fluid sub-problem.

Remark 3.7. In [13], the block Gauss-Seidel preconditioned Krylov subspace and the fully coupled FSI AMG methods are proposed, which are based on the smoothed aggregation multigrid method for each sub-problem, employed either in the preconditioning step or in the smoothing step.

Summarizing, compared to the others, we propose a preconditioner for the linearized FSI system, based on the complete LDU factorization of the reordered 3×3 system block matrix. The Schur complement itself corresponds to a fluid sub-problem, perturbed by a sparse matrix coming from the multiplication of the corresponding coupling matrices from the mesh movement, fluid and structure sub-problems, that is approximated and constructed in an explicit way.

4. NUMERICAL EXPERIMENTS

In this Section, we would like to demonstrate the robustness of the preconditioner in the preconditioned GMRES and flexible preconditioned GMRES methods for solving the FSI problem. For this reason, we test the algorithm for the FSI problem on three consecutively refined finite element meshes. We compare the iteration numbers of the preconditioned Krylov subspace methods, with varying mesh size, fluid density, and time step size.

4.1. Geometry, meshes, material parameters and boundary conditions. First we describe the geometry for the FSI simulation in Fig. 2. The channel has an obstacle inside, where the x -, y - and z -coordinates represent the lateral, anterior-posterior, and the vertical directions, respectively. The channel has the size $[0, 12]$ cm, $[0, 2]$ cm and $[0, 2]$ cm, in the x -, y - and z -direction, respectively. The obstacle is composed of four quarter cylinders with radius 0.8 cm, and two cubes inserted in between. The FSI interaction occurs on the obstacle surface inside the channel, when the flow goes from the left to right in the lateral direction. The finite element meshes are generated using Netgen

[34], where the conforming grids on the interface are guaranteed, see a mesh example in Fig.3. The information concerning the number of nodes ($\#Nod$), tetrahedral elements ($\#Tet$), and degrees of freedom ($\#Dof$) on the coarse mesh (C), intermediate mesh (I) and fine mesh (F) is summarized in Table 2.

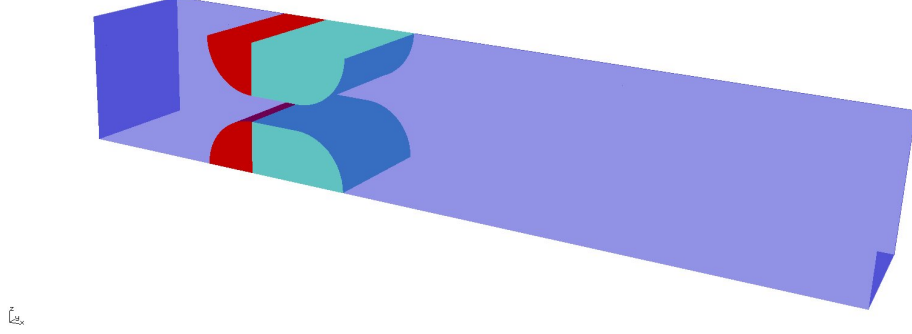


FIGURE 2. The configuration of the geometry.

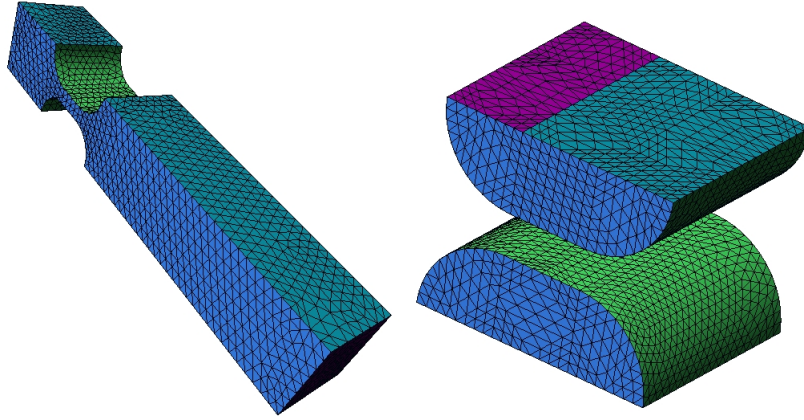


FIGURE 3. The mesh generated for the fluid domain (left) and the structure domain (right).

	$\#Nod$	$\#Tet$	$\#Dof$
Coarse mesh (C)	837	2679	5131
Intermediate mesh (I)	5002	21432	31178
Fine mesh (F)	34041	171456	214223

TABLE 2. Three finite element meshes.

We use the nonlinear isotropic and homogeneous hyperelastic model of the St. Venant Krichhoff material, where the elastic constants in (2) are $\lambda_s = 1.73\text{e}+06$ dyne/cm² and $\mu_s = 1.15\text{e}+06$ dyne/cm². The density of the structure is $\rho_s = 1$ g/cm³. The fluid kinematic viscosity is $\nu = 0.1568$ cm²/s. The fluid density is $\rho_f \in \{1.1, 0.11, \dots, 0.00011\}$ g/cm³ for our testing purpose, that covers a large range of flows, e.g., the water, blood and air flow. Note that, for numerical studying purpose, we successively decrease the fluid densities by factor of 10.

The structure is fixed on the boundaries except that part of the top and bottom in the vertical directions is assigned a homogeneous Neumann boundary condition as indicated by the purple color in Fig.3. The inflow boundary condition is $u = 30$ cm/s on Γ_{in} . For the outflow on Γ_{out} , we use "doing-nothing" condition, i.e., homogeneous Neumann boundary condition. On Γ_{wall} , we use homogeneous Dirichlet boundary condition. For testing purpose, we use the time step size $\Delta t \in \{1.25, 0.125, \dots, 0.00125\}$ ms.

4.2. Numerical studies on the robustness with respect to fluid density, mesh size and time step size. To study the robustness of the preconditioned Krylov subspace methods with respect to the varying fluid density, mesh size and time step size, we test the algorithm on three meshes (see Table. 2), with different fluid densities $\rho_f \in \{1.1, 0.11, \dots, 0.00011\}$ g/cm³, and different time step size $\Delta t \in \{1.25, 0.125, \dots, 0.00125\}$ ms. We uses the preconditioned GMRES and flexible GMRES as the outer acceleration. The iteration numbers of the preconditioned Krylov subspace methods are prescribed in Table 3 – 6, for solving the linearized FSI system at the first Newton iteration on the first time step. For other Newton iterations and time steps, we observe very similar results.

ρ_f	#it														
	1.1			0.11			0.011			0.0011			0.00011		
	C	I	F	C	I	F	C	I	F	C	I	F	C	I	F
Pre_GMRES	7	13	18	6	11	17	5	10	14	4	8	12	3	6	9
Pre_FGMRES	5	21	18	6	22	38	6	22	38	6	22	38	6	22	38

TABLE 3. The iteration numbers of the preconditioned GMRES and flexible GMRES with the time step size $\Delta t = 1.25$ ms.

ρ_f	#it														
	1.1			0.11			0.011			0.0011			0.00011		
	C	I	F	C	I	F	C	I	F	C	I	F	C	I	F
Pre_GMRES	3	5	8	3	5	8	3	5	5	2	4	5	2	4	5
Pre_FGMRES	3	7	8	4	8	12	4	9	14	4	9	15	4	9	15

TABLE 4. The iteration numbers of the preconditioned GMRES and flexible GMRES with the time step size $\Delta t = 0.125$ ms.

ρ_f	#it														
	1.1			0.11			0.011			0.0011			0.00011		
	C	I	F	C	I	F	C	I	F	C	I	F	C	I	F
Pre_GMRES	4	4	4	4	5	4	4	5	4	3	4	3	3	4	3
Pre_FGMRES	6	6	5	6	7	6	6	8	7	6	8	7	6	8	7

TABLE 5. The iteration numbers of the preconditioned GMRES and flexible GMRES with the time step size $\Delta t = 0.0125$ ms.

ρ_f	#it														
	1.1			0.11			0.011			0.0011			0.00011		
	C	I	F	C	I	F	C	I	F	C	I	F	C	I	F
Pre_GMRES	4	5	4	4	5	5	4	5	5	3	4	4	3	4	4
Pre_FGMRES	5	6	6	6	7	7	6	8	8	6	8	8	6	8	8

TABLE 6. The iteration numbers of the preconditioned GMRES and flexible GMRES with the time step size $\Delta t = 0.00125$ ms.

The observations are summarized in the following. We observe, that the preconditioned GMRES (Pre_GMRES) method performances better than the preconditioned flexible GMRES (Pre_FGMRES) method for our testing problem, i.e., the latter needs more iterations for all the test cases. The gap becomes smaller when the time step size is refined. Furthermore, the later shows to be more sensitive to the fluid density changes, i.e., when the density decreases, the iteration numbers very

slightly increase. However, for the Pre_GMRES method, we need fewer iterations when the fluid density decreases. In addition, as well known, when $\rho_f = \mathcal{O}(\rho_s)$ (in our case, $\rho_f \approx \rho_s = 1 \text{ g/cm}^3$), the so-called added-mass (see, e.g., [25]) plays important effect to the normal partitioned FSI solvers, that are usually become slow in such a situation; see [8]. However, our preconditioner shows the robustness with respect to such added-mass effect; see the iteration numbers corresponding to $\rho_f = 1.1 \text{ g/cm}^3$ in Table 4 – 6.

In any case, we need much fewer iterations than the results in Table 1 using the old preconditioners, i.e., our new preconditioner is much more efficient than the old ones with respect to the varying fluid densities. By this means, we overcome the robustness issues related to the fluid density using the old preconditioners.

Concerning the mesh dependence, from the results in Table 3, we see slightly increased iterations with the mesh refinement (C-I-F) for both methods. However, from the results in Table 4 – 6 with reduced time step size, we observe almost the same iterations on the three mesh levels for each method. Compared to the results in [23] using the old preconditioners, these new results demonstrate the more robustness of our new preconditioner with respect to the mesh size.

Furthermore, regarding the dependence on the time step size, except the result in Table 3, where a large time step size $\Delta t = 1.25 \text{ ms}$ is used in order to test the algorithm, that is usually much larger than required in the real simulation, we observe more or less similar iterations in Table 4 – 6, for a large range of time step size in each method. So, our new preconditioner shows the robustness with respect to the time step size.

We emphasize that, nearly the same complexity of the preconditioning step in the new preconditioner is needed in comparison with the old preconditioners \tilde{P}_{SSOR} and \tilde{P}_{ILU} . However, the iteration numbers of the Krylov subspace methods with the new preconditioner are approximately reduced by a factor of 10, see Table 1 and Table 4.

4.3. Visualization of the numerical solutions. To illustrate the numerical solutions, we plot the streamlines of the velocity fields behind the obstacles and the structure deformations from the FSI simulation using different density $\rho_f = 1.1 \text{ g/cm}^3$ (close to water) and $\rho_f = 0.0011 \text{ g/cm}^3$ (close to air) in Fig. 4 and Fig. 5, respectively. The simulation results at different time level $t \in \{0.125, 7, 14.5\} \text{ ms}$ and $t \in \{0.125, 14.5, 40.5\} \text{ ms}$ are shown from top to bottom in Fig. 4 and Fig. 5, respectively. For visualization purpose, the deformation of the structure body is enlarged by a factor of 10. We observe larger structure deformation in the FSI simulation with $\rho_f = 1.1 \text{ g/cm}^3$ than

with $\rho_f = 0.0011 \text{ g/cm}^3$. In addition, we also observe some vorticities behind the obstacle at late time level, e.g., at $t = 14.5 \text{ ms}$ for $\rho_f = 1.1 \text{ g/cm}^3$ and $t = 40.5 \text{ ms}$ for $\rho_f = 0.0011 \text{ g/cm}^3$. From the numerical experiments, we also observe, that the velocity speed of the air flow reaches much higher level than the water flow at the very first time step.

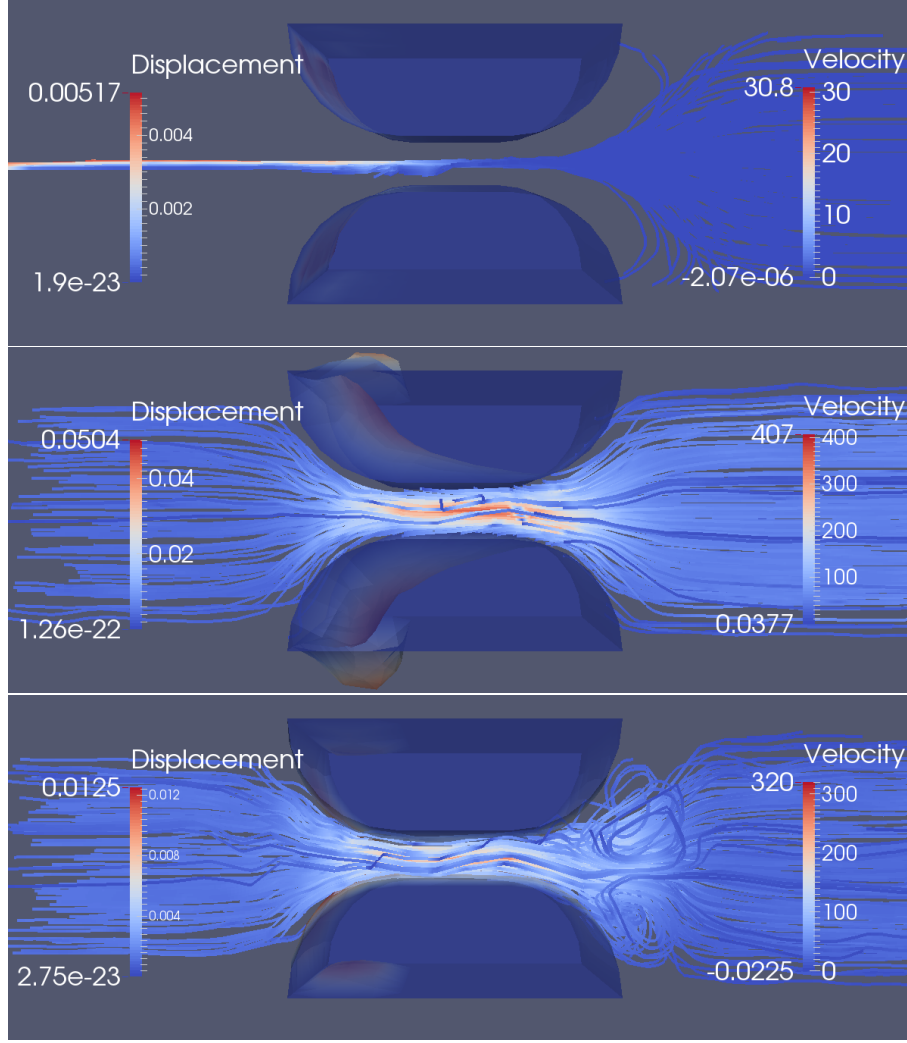


FIGURE 4. The fluid velocity and structure displacement fields of the FSI simulation with $\rho_f = 1.1 \text{ g/cm}^3$ at different time levels: $t = 0.125 \text{ ms}$, $t = 7 \text{ ms}$ and $t = 14.5 \text{ ms}$ (from top to bottom).

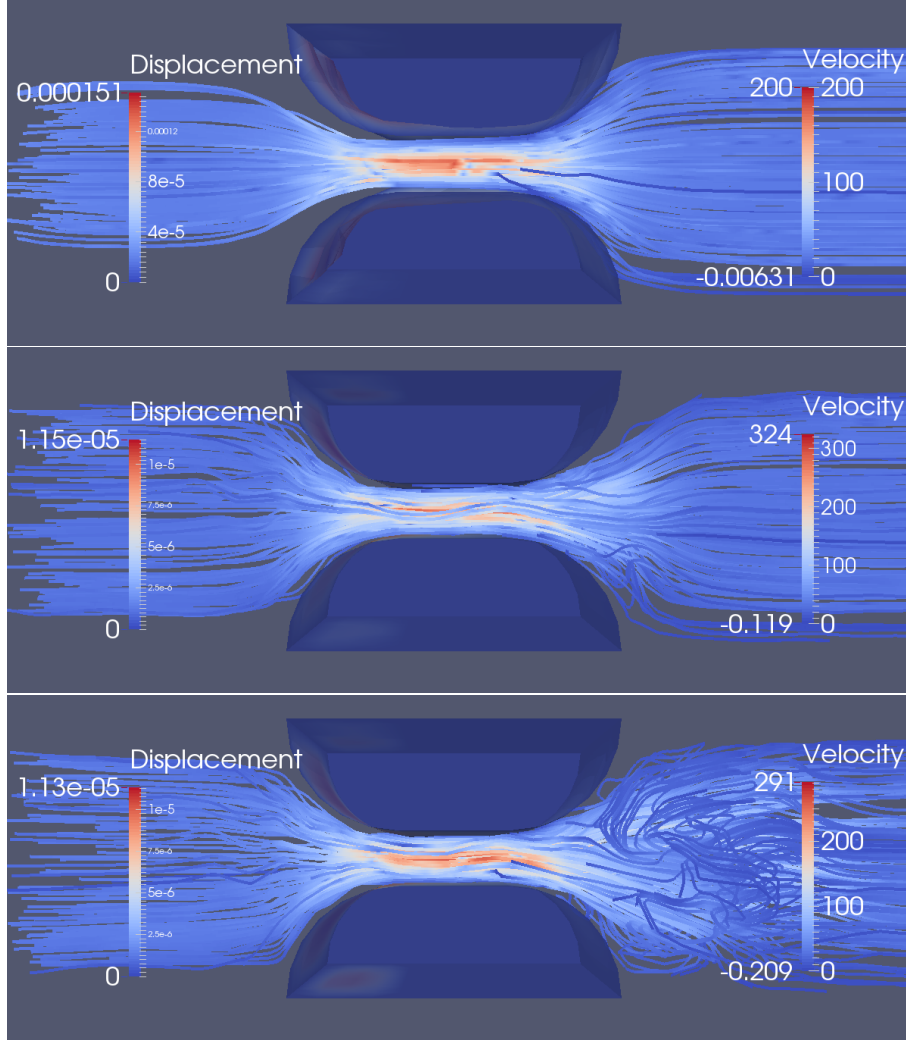


FIGURE 5. The fluid velocity and structure displacement fields of the FSI simulation with $\rho_f = 0.0011 \text{ g/cm}^3$ at different time levels: $t = 0.125 \text{ ms}$, $t = 14.5$ and $t = 40.5 \text{ ms}$ (from top to bottom).

5. CONCLUSIONS

In this work, we develop a new preconditioner for the coupled FSI system of finite element equations based on the proper approximation of the complete *LDU* factorization of the system matrix. From our numerical studies, the preconditioner shows the more robustness with respect to the mesh size, varying fluid density, and in addition, to the time step size, without resorting to the more involved fully coupled FSI

monolithic multigrid methods. Thus, the new method may reduce the implementation and computational complexity significantly.

REFERENCES

- [1] A. APOSPORIDIS, P. S. VASSILEVSKI, AND A. VENEZIANI, *Multigrid preconditioning of the non-regularized augmented Bingham fluid problem*, Electron. Trans. Numer. Anal., 41 (2014), pp. 42–61.
- [2] O. AXELSSON AND P. S. VASSILEVSKI, *Algebraic multilevel preconditioning methods. I*, Numer. Math., 56 (1989), pp. 157–177.
- [3] ———, *Algebraic multilevel preconditioning methods, II*, SIAM J. Numer. Anal., 27 (1990), pp. 1569–1590.
- [4] S. BADIA, A. QUAINI, AND A. QUARTERONI, *Modular vs. non-modular preconditioners for fluid-structure systems with large added-mass effect*, Comput. Methods Appl. Mech. Engrg., 197 (2008), pp. 4216–4232.
- [5] S. BADIA, A. QUAINI, AND A. QUARTERONI, *Splitting methods based on algebraic factorization for fluid-structure interaction*, SIAM J. Sci. Comput., 30 (2008), pp. 1778–1805.
- [6] A. BARKER AND X. CAI, *Scalable parallel methods for monolithic coupling in fluid-structure interaction with application to blood flow modeling*, J. Comput. Phys., (2010), pp. 642–659.
- [7] J. BONET AND R. WOOD, *Nonlinear Continuum Mechanics for Finite Element Analysis*, Cambridge University Press, New York, 2008.
- [8] P. CAUSIN, J. GERBEAU, AND F. NOBILE, *Added-mass effect in the design of partitioned algorithms for fluid-structure problems*, Comput. Methods Appl. Mech. Engrg., 194 (2005), pp. 4506–4527.
- [9] P. CROSETTO, S. DEPARIS, G. FOURESTY, AND A. QUARTERONI, *Parallel algorithms for fluid-structure interaction problems in haemodynamics*, SIAM J. Sci. Comput., 33 (2011), pp. 1598–1622.
- [10] J. DONEA, A. HUERTA, J. PONTOT, AND A. FERRAN, *Arbitrary Lagrangian-Eulerian methods*, in The Encyclopedia of Computational Mechanics, E. Stein, R. Borst, and T. Hughes, eds., vol. 1, Wiley& Sons, Ltd, 2004, pp. 413–437.
- [11] H. ELMAN, *Preconditioning for the steady-state Navier–Stokes equations with low viscosity*, SIAM J. Sci. Comput., 20 (1999), pp. 1299–1316.
- [12] L. FORMAGGIA AND F. NOBILE, *A stability analysis for the arbitrary Lagrangian Eulerian formulation with finite elements*, East-West J. Numer. Math., 7 (1999), pp. 105–132.
- [13] M. W. GEE, U. KTTLER, AND W. A. WALL, *Truly monolithic algebraic multigrid for fluidstructure interaction*, Int. J. Numer. Meth. Engrg., 85 (2011), pp. 987–1016.
- [14] G. HAASE AND U. LANGER, *Modern Methods in Scientific Computing and Applications*, vol. 75 of NATO Science Series II. Mathematics, Physics and Chemistry, Kluwer Academic Press, Dordrecht, 2002, ch. Multigrid Methods: From Geometrical to Algebraic Versions, pp. 103–154.
- [15] W. HACKBUSCH, *Multi-Grid Methods and Applications*, Springer, Berlin, 2003.
- [16] M. HEIL, *An efficient solver for the fully coupled solution of large-displacement fluid-structure interaction problems*, Comput. Methods Appl. Mech. Engrg., 193 (2004), pp. 1–23.

- [17] G. HOLZAPFEL, *Nonlinear Solid Mechanics: A Continuum Approach for Engineering*, John Wiley & Sons, Chichester, 2000.
- [18] J. HRON AND S. TUREK, *A monolithic FEM/Multigrid solver for an ALE formulation of fluid-structure interaction with applications in biomechanics*, in Fluid-Structure Interaction, H.-J. Bungartz and M. Schäfer, eds., vol. 53 of Lecture Notes in Computational Science and Engineering, Springer, 2006, pp. 146–170.
- [19] T. HUGHES, W. LIU, AND T. ZIMMERMANN, *Lagrangian-Eulerian finite element formulation for incompressible viscous flows*, Comput. Methods Appl. Mech. Engrg., 29 (1981), pp. 329–349.
- [20] M. JUNG AND U. LANGER, *Application of multilevel methods to practical problems*, Surv. Math. Ind., 1 (1991), pp. 217–257.
- [21] F. KICKINGER, *Algebraic multigrid for discrete elliptic second-order problems*, in Multigrid Methods V. Proceedings of the 5th European Multigrid conference (ed. by W. Hackbush), Lecture Notes in Computational Sciences and Engineering, vol. 3, Springer, 1998, pp. 157–172.
- [22] J. KRAUS AND S. MARGENOV, *Robust Algebraic Multilevel Methods and Algorithms*, vol. 5 of Radon Series on Computational and Applied Mathematics, Walter de Gruyter, Berlin, New York, 2009.
- [23] U. LANGER AND H. YANG, *Numerical simulation of fluid-structure interaction problems with hyperelastic models: A monolithic approach*, arXiv:1408.3737, (2014).
- [24] U. LANGER AND H. YANG, *Partitioned solution algorithms for fluid-structure interaction problems with hyperelastic models*, J. Comput. Appl. Math., 276 (2015), pp. 47–61.
- [25] H.-P. MORAN AND R. OHAYON, *Fluid-Structure Interaction: Applied Numerical Methods*, John Wiley & Sons, 1995.
- [26] R. L. MUDDLE, M. MIHAJLOVIĆ, AND M. HEIL, *An efficient preconditioner for monolithically-coupled large-displacement fluid-structure interaction problems with pseudo-solid mesh updates*, J. Comput. Phys., 231 (2012), pp. 7315–7334.
- [27] Y. NOTAY AND P. S. VASSILEVSKI, *Recursive Krylov-based multigrid cycles*, Numer. Linear Algebra Appl., 15 (2008), pp. 473–487.
- [28] A. QUARTERONI AND A. VALLI, *Domain Decomposition Methods for Partial Differential Equations*, Oxford Sciences Publications, 1999.
- [29] M. RAZZAQ, H. DAMANIK, J. HRON, A. OUAZZI, AND S. TUREK, *FEM multigrid techniques for fluidstructure interaction with application to hemodynamics*, Appl. Numer. Math., 62 (2012), pp. 1156–1170.
- [30] J. W. RUGE AND K. STÜBEN, *Algebraische mehrgittermethoden (AMG)*, in Multigrid Methods, vol. 3 of Frontiers in Applied Mathematics, SIAM, Philadelphia, 1987, pp. 73–130.
- [31] Y. SAAD, *A flexible inner-outer preconditioned GMRES algorithm*, SIAM J. Sci. Comput., 14 (1993), pp. 461–469.
- [32] Y. SAAD, *Iterative Methods for Sparse Linear Systems*, SIAM, Philadelphia, 2003.
- [33] Y. SAAD AND M. H. SCHULTZ, *GMRES: A generalized minimal residual algorithm for solving nonsymmetric linear systems*, SIAM J. Sci. Stat. Comput., 7 (1986), pp. 856–869.

- [34] J. SCHÖBERL, *NETGEN - An advancing front 2D/3D-mesh generator based on abstract rules*, Comput Visual Sci, 1 (1997), pp. 41–52.
- [35] A. TOSELLI AND O. WIDLUND, *Domain Decomposition Methods-Algorithms and Theory*, Springer, Heidelberg, 2005.
- [36] S. TUREK, *Efficient Solvers for Incompressible Flow Problems*, Springer, Berlin, 1999.
- [37] P. S. VASSILEVSKI, *Multilevel Block Factorization Preconditioners*, Springer, Heidelberg, 2008.
- [38] M. WABRO, *Coupled algebraic multigrid methods for the Oseen problem*, Comput. Visual. Sci., 7 (2004), pp. 141–151.
- [39] ———, *AMGe—coarsening strategies and application to the Oseen equations*, SIAM J. Sci. Comput., 27 (2006), pp. 2077–2097.
- [40] T. WICK, *Fluid-structure interactions using different mesh motion techniques*, Comput. Structures, 89 (2011), pp. 1456–1467.
- [41] T. A. WIESNER, R. S. TUMINARO, W. A. WALL, AND M. W. GEE, *Multigrid transfers for nonsymmetric systems based on Schur complements and Galerkin projections*, Numer. Linear Algebra Appl., 21 (2014), pp. 415–438.
- [42] H. YANG, *Partitioned solvers for the fluid-structure interaction problems with a nearly incompressible elasticity model*, Comput. Visual. Sci., 14 (2011), pp. 227–247.
- [43] H. YANG AND W. ZULEHNER, *Numerical simulation of fluid-structure interaction problems on hybrid meshes with algebraic multigrid methods*, J. Comput. Appl. Math., 235 (2011), pp. 5367–5379.

JOHANN RADON INSTITUTE FOR COMPUTATIONAL AND APPLIED MATHEMATICS (RICAM), AUSTRIAN ACADEMY OF SCIENCES, ALTENBERGER STRASSE 69, A-4040 LINZ, AUSTRIA

E-mail address: `ulrich.langer@ricam.oeaw.ac.at`

URL: `http://www.ricam.oeaw.ac.at/people/u.langer/`

JOHANN RADON INSTITUTE FOR COMPUTATIONAL AND APPLIED MATHEMATICS (RICAM), AUSTRIAN ACADEMY OF SCIENCES, ALTENBERGER STRASSE 69, A-4040 LINZ, AUSTRIA

E-mail address: `huidong.yang@oeaw.ac.at`

URL: `http://people.ricam.oeaw.ac.at/h.yang/`